NUMERICAL SIMULATION OF FOCUSED WAVE IMPACT ON A 2-D FLOATING STRUCTURE

X.Z. Zhao [12]

ABSTRACT: Freak (Extreme, rogue) waves are extremely large water waves in ocean and may occur all over the world sea area. Such a wave may lead to damage of coastal and offshore structures. Accurate prediction of extreme wave-induced forces and motions is of importance and necessaries for researchers and engineers for the purpose of structure design and disaster prevention. Due to the complexity of nonlinear wave-structure interactions related with distorted free surface and relatively large amplitude of structure response, a great deal of effort is required to investigate the physics. Here, a Computational Fluid Dynamics (CFD) model has been developed to study focused wave impact on a floating structure and validated by a newly designed experiment. Focused waves are generated based on the mechanism of wave focusing in a two-dimensional wave tank. In the experiment, a model of a box-shaped floating body with a small freeboard is adopted in order to easily obtain green water phenomena. The computations are performed by a Constrained Interpolation Profile (CIP)-based Cartesian grid method. The CIP algorithm is adopted as the base scheme to obtain a robust flow solver of the Navier-stokes equation with free surface boundary. An improved THINC scheme (THINC, tangent of hyperbola for interface capturing), the more accurate THINC/SW scheme (THINC with Slope Weighting), is applied as the free surface/ interface capturing method. Main attentions are paid to the three degrees of freedom (3-DOF) body motions, pressure domain around the structure and nonlinear phenomena, such as water on deck. The highly nonlinear wave-structure interactions, including significant body motion and water on deck, are modeled successfully in comparison with experimental measurements. It is concluded that the present model with the aid of the CIP technique can provide with acceptably accurate numerical results on the route to practical purposes.

Keywords: Freak wave; vof; floating body; water on deck; thinc/sw method

INTRODUCTION

A great number of research interests on freak waves have been widely motivated since the stories of monstrous waves have been told by sailors (Draper, 1965). Resently, Nikolkina and Didenkulova (2011) collected the evidence of rogue wave events all over the world during past five years (2006-2010). It is found that the waves occurred not only in deep and shallow zones of the world ocean seas, but also at the coast, where they are manifested as either sudden flooding of the coast or high splashes over steep banks or sea walls. Investigation on the formation of very large water waves has been studied extensively in the past several decades ever since Longuet-Higgins (1952) first investigated the statistics of extreme waves in narrow-banded random wave field. Numerous studies have shown that the extreme wave occurrence may be related with wave energy focusing including a number of factors: wave-wave interactions, wave-current interactions, bathymetry, wind effect, self-focusing instabilities, directional effects, etc. More details on these different mechanisms of extreme wave formation have been reviewed by Kharif and Pelinovsky (2003) and Dysthe et al. (2008). The wave focusing approach is one of the most powerful methods with a controlled focusing both in time and space. Since it has been firstly proposed by Davis and Zarnick (1964), then for example applied in different studies by Huang and Lin (2012) and Zhao et al. (2009; 2010a; 2010b). However, they paid their attentions on the features of the extreme wave profile. Seldom was about extreme waves interacting with bodies or floating bodies. Liu et al. (2010) and Li et al. (2012) investigated the 2-D phase focusing wave and 3-D multi-directional focused wave run-up on a bottom-founded vertical cylinder in an experimental flume. Zang et al. (2010) reported on the interaction of steep waves, both non-breaking and breaking, hitting a bottom-founded vertical circular cylinder in a physical wave flume. Westphalen et al. (2012) dealt with the generation and behavior of extreme focused wave groups and the corresponding forces on horizontal and vertical cylinders in a numerical wave tank. Hu et al. (2011) using an in-house CFD flow code studied the wave loading on a wave energy converter (WEC) device in heave motion.

[1] Ocean College, Zhejiang University, No.866 Yuhangtang Road, Hangzhou, 310058, CHINA
[2] State Key Laboratory of Satellite Ocean Environment Dynamics, the second Institute of Oceanography, No.36 baochubei Road, Hangzhou, 310012, CHINA

The nonlinear distorted free surface associated with focused wave impact as nonlinearity is one of its main characteristic features. Among the available strategies to numerically construct an interface, the VOF method is one of the most popular in water-surface capturing, first introduced by Hirt and Nichols (1981). After that, many improved VOF schemes have been proposed, like PLIC-VOF (Young 1982), THINC (Xiao et al. 2005), THINC/WLIC (Yokoi 2007) (WLIC: weighed line interface calculation) and THINC/SW scheme (Xiao et al. 2011). In this paper, the THINC/SW scheme is combined with the CIP-based model to treat the violent free surface.

The CIP-based model for free-surface flow problems was proposed by Hu and Kashiwagi (2004), where a CIP method was introduced to obtain a robust flow solver of Navier-Stokes equations and also for the free surface treatment.. The CIP method is a compact upwind scheme with sub-cell resolution for the advection calculation proposed by Yabe et al. (2001). In the CIP method, both the advection function and its spatial derivatives are used to construct an interpolation approximation of high accuracy within one grid cell. Since the spatial derivatives are also employed, the interface profile inside the grid is retrieved, and the sub-cell resolution can be obtained. Hu and Kashiwagi (2009) presented an enhanced model for nonlinear wave-body interactions, in which the THINC scheme was combined to the model. Recently, Zhao (2011) applied the CIP-based model to free surface flow problems. Main attentions were focused on the surface profiles of dam break and water waves. Zhao and Hu (2012) presented an enhanced model to treat body motions due to extreme waves, in which the THINC/WLIC scheme was introduced for the free surface capturing. They paid attentions to the 2-DOF body motions. However, 3-DOF body motions were not presented.

The objective of this paper is to study the violent impact on a 2-D freely floating structure due to focused waves. 2-DOF body motions have been studied previously (Zhao and Dong, 2011). In this study, a multi-phase flow model, which solves the flow in the air, water and solid simultaneously, has been applied to study the 3-DOF body motions due to focused waves. In the remainder of this paper, we introduce briefly the numerical implementations for the governing equations and the free surface representations. An improved interface capturing method, THINC/SW method is outlined. Then, the experimental set-up is presented. Finally, the computational results are presented about the interaction between focused waves and a floating body. Main attentions are paid to the structure response, green water impact pressure, and the velocity field around the structure. The article closes with some general conclusions on the present work.

CFD MODEL

The computations reported here are carried out by using a CIP-based model (Zhao and Hu 2012) for dealing with strongly nonlinear wave-structure interactions. The method is built based on the solution of the Navier-Stokes equations with the CIP method adopted as the base numerical scheme to obtain a robust flow solver in a Cartesian grid, where the THINC/SW (Xiao et al. 2011) scheme is used for free surface/interface capturing; and an immersed boundary method for the coupling of wave-structure interaction.

Considering flows of an incompressible fluid with the free surface, the governing equations are the continuity equation and the Navier-Stokes equations as follows:

$$\frac{\partial u_i}{\partial x_i} = 0 \tag{1}$$

$$\frac{\partial u_i}{\partial t} + u_j \frac{\partial u_i}{\partial x_j} = -\frac{1}{\rho}\frac{\partial p}{\partial x_i} + F_i + \frac{1}{\rho}\frac{\partial}{\partial x_j}\left(2\mu S_{ij}\right) \tag{2}$$

where u_i, i=1, 2 are the velocity components along the coordinate axes x_i; t is time; p is hydrodynamic pressure; $S_{ij}=(\partial u_i/\partial x_j+\partial u_j/\partial x_x)/2$; □ and □ are the water density and viscosity, respectively. The second term on the right-hand of Eq. (2) is the external force, including the gravitational force. The pressure-velocity coupling is treated in a non-advection step calculation, in which the following Poisson equation is solved.

$$\frac{\partial}{\partial x_i}\left(\frac{1}{\rho}\frac{\partial p^{n+1}}{\partial x_i}\right) = \frac{1}{\Delta t}\frac{\partial u_i^{**}}{\partial x_i} \tag{3}$$

Equation (4) is assumed to be valid for liquid, gas and solid phase.

In the model, the fluid-body interaction is considered as a multi-phase problem that includes water, air and structure. A fixed Cartesian grid that covers the whole computation domain is used. A volume fraction field ϕ_m (m=1, 2, and 3 indicate water, air and solid, respectively) is used to represent and track the interface. The total volume function for water and structure is solved by using the following advection equation.

$$\frac{\partial \phi_{13}}{\partial t} + \vec{u}\cdot\nabla\phi_{13} = 0 \tag{4}$$

Here, $\phi_{13} = \phi_1 + \phi_3$. The density and viscosity of the solid phase are treated as the same as those of a liquid phase to ensure computation stability. The volume function for solid body ϕ_3 is determined by a Lagrangian method in which a rigid body is assumed (Hu and

Kashiwagi, 2009). The position of water is calculated by $\phi_1=\phi_{13}-\phi_3$, where the position of liquid and solid phase ϕ_{13} is captured by a free surface/interface capturing method. The volume function for air ϕ_2 is then determined by $\phi_2 = 1.0-\phi_1-\phi_3$. After all volume functions have been calculated, the physical property λ, such as the density ρ and viscosity μ, are calculated by the following formula.

$$\lambda = \sum_{m=1}^{3} \phi_m \lambda_m \tag{5}$$

The drawback of the averaging process is that the computational accuracy is reduced to first order in terms of cell size at the interfaces.

FREE SURFACE METHOD

In a physical problem the gas-liquid interface (free surface) is with zero thickness. However when we solve the density function of liquid ϕ_1 by Eq. (4), we obtain a free surface with finite thickness, i.e., a smeared interface due to numerical diffusion associated with the finite difference scheme. To avoid this, we use an accurate interface capturing scheme, the THINC/SW scheme (Xiao et al., 2011) to calculate the free surface. The THINC/SW scheme is also a VOF (Hirt and Nichols 1981) type method. In the THINC/SW method, a variable steepness parameter is adopted instead of the constant steepness parameter that used in the original THINC scheme (Xiao et al. 2005), which helps maintain the thickness of the jump transition layer. A 1-D THINC scheme is described in the following.

The one-dimensional advection equation for a density function ϕ can be written in conservation form as follows:

$$\frac{\partial \phi}{\partial t} + \nabla(u\phi) = \phi \frac{\partial u}{\partial x} \tag{6}$$

Equation (6) is descretized by a finite volume method. For a known velocity field u^n, integrating Eq. (6) over a computational cell $[x_{i-1/2}, x_{i+1/2}]$ and a time interval $[t^n, t^{n+1}]$ we have:

$$\bar{\phi}_i^{n+1} = \bar{\phi}_i^n + \frac{1}{\Delta x_i}\left(g_{i-1/2} - g_{i+1/2}\right) + \frac{\Delta t}{\Delta x_i}\bar{\phi}_i^n\left(u_{i+1/2}^n - u_{i-1/2}^n\right) \tag{7}$$

Where $\Delta x_i = x_{i+1/2} - x_{i-1/2}$, $\Delta t = t^{n+1} - t^n$, $g_{t\pm\frac{1}{2}} = \int_{t^n}^{t^{n+1}} (u\phi)dt$ is the flux across the cell boundary ($x=x_{i\pm1/2}$), and $\bar{\phi} = \frac{1}{\Delta x}\int_{x_{i-1/2}}^{x_{i+1/2}} \phi(x,t)dx$ is the cell-averaged density function defined at the cell center($x=x_i$). The fluxes are calculated by a semi-Lagrangian method. Similar to the CIP method, the profile of □ inside an upwind computation cell is approximated by an interpolation function. Instead of using a polynomial in the CIP scheme, the THINC scheme uses a hyperbolic tangent function in order to avoid numerical smearing and oscillation at the interface. Since $0 \le \chi \le 1$, and the variation of χ αacross the free surface is step-like, a piecewise modified hyperbolic tangent function is used to approximate the profile inside a computation cell, which is shown as follows:

$$\chi_{x,i} = \frac{\alpha}{2}\left\{1 + \gamma \tanh\left[\beta\left(\frac{x - x_{i-1/2}}{\Delta x_i} - \delta\right)\right]\right\} \tag{8}$$

where $\alpha, \gamma, \delta, \beta$ are parameters to be specified. α and γ are a parameter used to avoid interface smearing, which are given as follows:

$$\alpha = \begin{cases} \bar{\phi}_{i+1} & \text{if } \bar{\phi}_{i+1} \ge \bar{\phi}_{i-1} \\ \bar{\phi}_{i-1} & \text{otherwise} \end{cases}, \gamma = \begin{cases} 1 & \text{if } \bar{\phi}_{i+1} \ge \bar{\phi}_{i-1} \\ -1 & \text{otherwise} \end{cases} \tag{9}$$

Parameter δ is used to determine the middle point of the hyperbolic tangent function, and is calculated by solving the following equation:

$$\frac{1}{\Delta x_i}\int_{x_{i-1/2}}^{x_{i+1/2}} \chi_i(x)dx = \bar{\phi}_i^n \tag{10}$$

Parameter β is used to control the sharpness of the variation of the color function. In the original THINC scheme, a constant β=3.5 is usually used which may result in ruffling the interface which aligns nearly in the direction of the velocity (Xiao et al. 2011). Therefore, a refined THINC scheme, the THINC/SW, by determining adaptively according to the orientation of the interface is proposed by Xiao et al. (2011).

In two-dimensional case, parameters β could be determined by the following equations:

$$\beta_x = 2.3|n_x| + 0.01,\ \beta_y = 2.3|n_y| + 0.01 \tag{11}$$

where $n=(n_x, n_y)$ is the unit norm vector of the interface.

After $\chi_i(x)$ is determined, the flux at the cell boundary can be calculated by Eq. 8. In Fig. 1, for $u_{i+1/2}>0$ is indicated by the dashed area. After all of the fluxes across the cell boundaries have been computed, the cell-integrated value at the new time step can be obtained by Eq. (7). This cell-integrated value is used to determine the free surface position; therefore, mass conservation is automatically satisfied for the liquid.

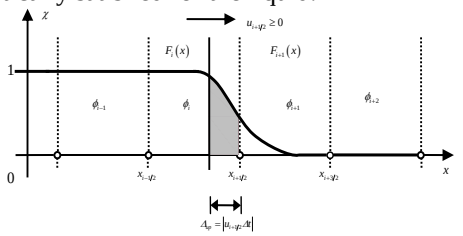

Fig. 1 Concept of the THINC/SW scheme

Laboratory experiments

The experiments were conducted in a narrow wave flume at Research Institute for Applied Mechanics (RIAM) Kyushu University. The glass-walled flume is

18m long, 0.3m wide and 0.7 m high and is equipped with a plunge-type wave generator at one end and a wave absorbing device at the other end. The schematic of the experimental set-up is shown in Fig. 2 and a photo of the floating body is shown in Fig. 3. The main model geometrical and hydrostatic information are summarized in table 1. The body is free to move in heave and roll with sway restrained by a spring. The allowed motions are measured by potentiometers. The structural design ensures negligible elastic deformations. The prescribed wave parameters are checked with wave gauges located along the flume with a 100Hz sampling frequency, while 1000Hz sampling frequency for the wave-body interactions. A pressure gauge is placed on the superstructure at a height of 0.01m from the deck, as shown in Fig. 5 to measure the green water impact pressure. The experiments are recorded by a high-speed camera for a qualitative understanding of the water-on-deck occurrence.

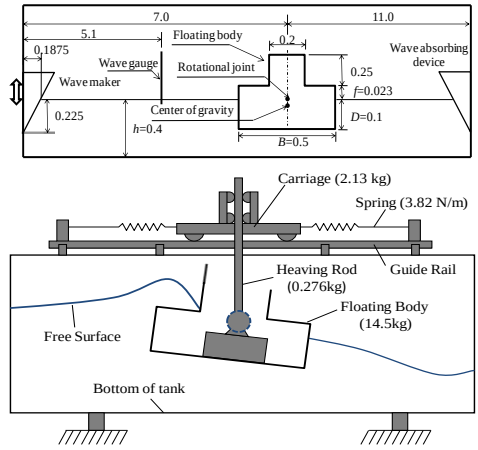

Fig. 2 Schematic of experimental setup (Unit: m)

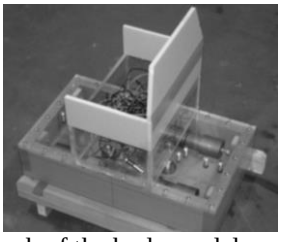

Fig. 3 Photograph of the body model used in this study

Table 1 main parameter of the body model

Item	Value(m)
Length	0.5
Breadth	0.29
Draft	0.10
Gyration radius	0.1535
Center of gravity (from the bottom)	0.0796

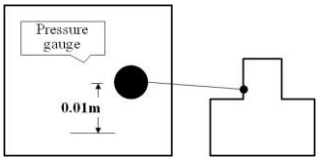

Fig. 4 Details of the pressure transducer.

RESULTS

Zalesak's problem

A validation test, known as Zalesak's problem (Zalesak, 1979), is performed with the THINC/SW scheme and the original THINC scheme. Three cases with different grid size are carried out. This test is one of the most popular scalar advection tests. A velocity field is given by $\mathbf{u} = (y-0.5,\ 0.5-x)$ with $\Delta t = 2\pi/628$. One revolution is completed in 628 time steps. Numerical error is defined as

$$\text{Error} = \sum_{i,j} \left| \phi_{i,j}^{n} - \phi_{i,j}^{ex} \right| \Big/ \sum_{i,j} \phi_{i,j}^{ex} \qquad (12)$$

Here, $\phi_{i,j}^{ex}$ is the exact solution of $\phi_{i,j}^{n}$. Table 1 shows the result of the numerical error. Shape distortion is evaluated in Fig. 5 after one rotation. The dotted contour line shows the exact shape and the solid contour line shows the computational solution. It can be seen from these figures and the table that a finer grid produces better shape retention and numerical error of the THINC/SW scheme is lower than the original THINC scheme. Therefore, the THINC/SW scheme is applied in the present flow solver for green water problem.

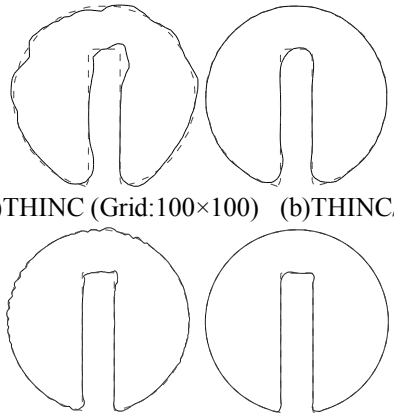

(a)THINC (Grid:100×100) (b)THINC/SW

(c)THINC (Grid:500×500) (d)THINC/SW

Fig. 5 Numerical results of Zalesak's problem after one rotation: (a, b:Grid: 100×100) (c, d:Grid: 100×100)

Table 2 Errors for Zalesak's test problem

Grid Number	100×100	500×500
THINC	9.11×10^{-2}	2.04×10^{-2}
THINC/SW	5.16×10^{-2}	1.01×10^{-2}

Wave generation

In order to obtain extreme waves, a relatively easy way is using wave focusing. The mechanism of two-dimensional wave focusing is related to the wave dispersion, i.e. dependence of the group velocity on the wave frequency. If during the initial moment the short waves having small group velocities are located in front of the long waves having large group velocities, then in the phase of development, long waves will overtake short waves, and a large amplitude wave can appear at some fixed time owing to the superposition of all the waves located at the same place. Then the extreme wave model is represented as

$$\eta(x,t)=\sum_{i=1}^{N_f} a_i \cos\left(k_i\left(x-x_p\right)-\omega_i\left(t-t_p\right)\right) \tag{13}$$

where a_i is the amplitude of component wave with the ith frequency ω_i, k_i the wavenumber and N_f is the number of wave components; x_p and t_p are focusing position and focusing time, respectively. In the present paper, the initial wave conditions are: the number of the wave components: N_f=29; wave frequency range: f (0.6, 1.6); the peak wave period T_p=1.2; focus position and time: x_p=7.0m, t_p=20s; the input wave amplitudes: A=0.07m; total time calculated up to t=30s. A JONSWAP spectrum is used to calculate the amplitudes of the individual wave components a_i

Prior to the simulations with the floating body, simulations without the body are performed to compare the undisturbed simulated wave elevation with the measured wave elevation in the empty flume. Fig. 6 displays the evolution of extreme wave along the wave flume resulting from the focus amplitude A_f=0.07m. The plots show numerical and measured time series of the free surface elevation and the results are presented for five wave gauges along the flume. The comparisons displayed in Fig. 5 show that the calculations agree well with the experimental data. For this case, it can be noticed that the crest is twice as much as the trough when the extreme wave happens, which is the main difference from regular wave of an even energy distribution.

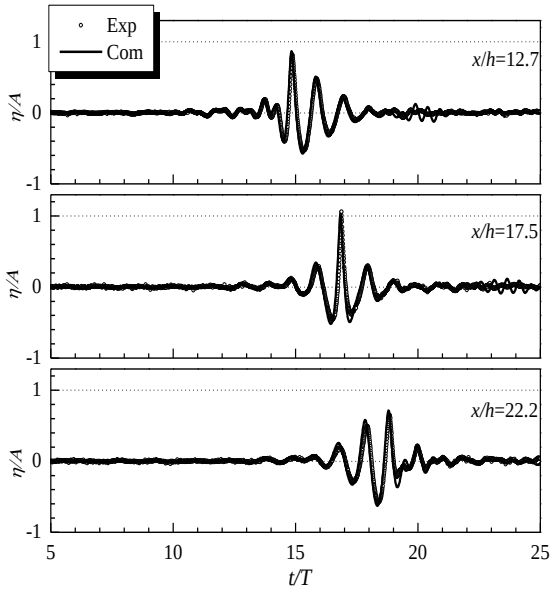

Fig. 6 Focused wave profile along the tank

2-DOF body motions

The aim of this paper is to estimate the efficiency of our numerical code to deal with large displacement of the body due to focused waves. In this section, 2-DOF body motions are considered. The carriage is fixed on the guide rails.

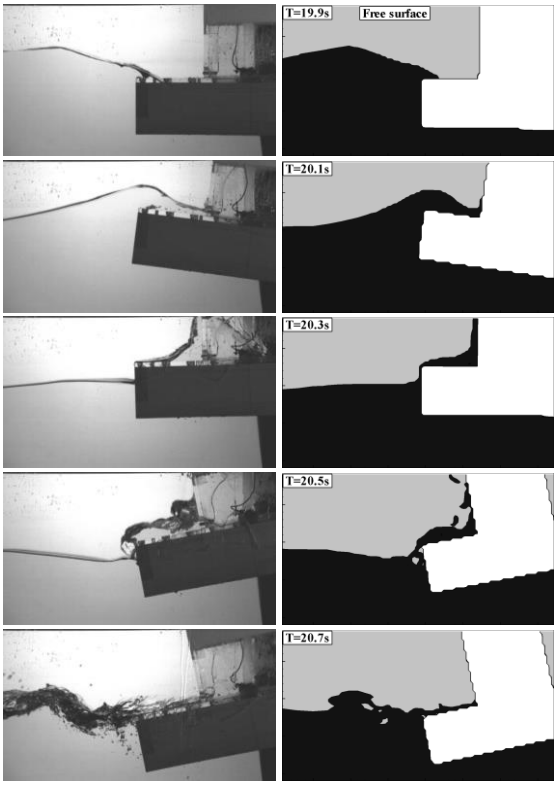

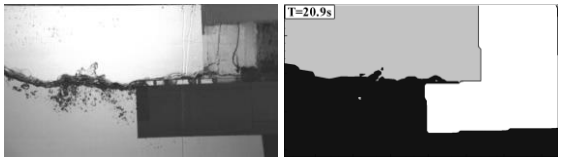

Fig. 7 Comparison of free surface and body position for focused wave: A_f=0.07m with sway motion fixed

Fig. 7 shows a clear numerical record of the extreme wave impact on the floating body with photographs from the experiment. Before the flow reaches the superstructure, a steep slope is generated at the front edge of the deck and the wave front collides with the superstructure. Because of the vertical wall, the wave front is deviated upward and is deflected to a vertical jet. It rises vertically up the wall and is slowed down by the gravity action. Finally, the fluid motion is converted into a water run-down by the gravity, and then overturns. This causes the formation of a backward plunging wave hitting the deck, striking the underlying water and entrapping air with a deep heave and roll motion. The comparison of the pressure time histories obtained at the pressure gage is plotted in Fig. 8, where solid line denotes numerical results, and dash line presents experimental measurements. All the pressure records show the presence of two main peaks. The first peak happens at the start of the water-on-deck run-up along the superstructure and corresponds to the initial impact of the liquid with the structure. The second peak occurs during the final stages of wave-body interactions. Cross-checking the pressure time histories with water-on-deck visualizations, it appears that the second peak pressure occurs during the water run-down phase. The second peak impact pressure reflects the fact the wave-on-deck overturns and collides with the superstructure again after it hits the deck. The largest second peak pressure is observed on the superstructure in the experiment, whereas that is not clear in the numerical simulation. The body motion caused by a focused wave is shown in Fig. 9. We can see that the floating body shows a large amplitude response subjected to the extreme wave, especially for the roll motion. The amplitude of the nonlinear oscillation in heave is still slightly underestimated, but the tendency in variation is successfully predicted compared to the physical experiment. The simulated large motion in roll is almost the same as the measured values, also the free surface elevation at x=5.1m. In despite of this phenomenon being one of the most violent forms of wave motion, these behaviors can be modeled in the computation comparing with the physical experiment.

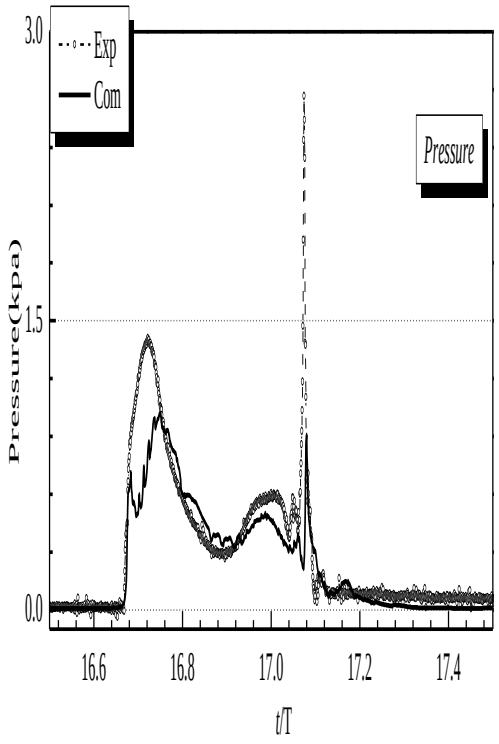

Fig. 8 Impact pressure due to green water

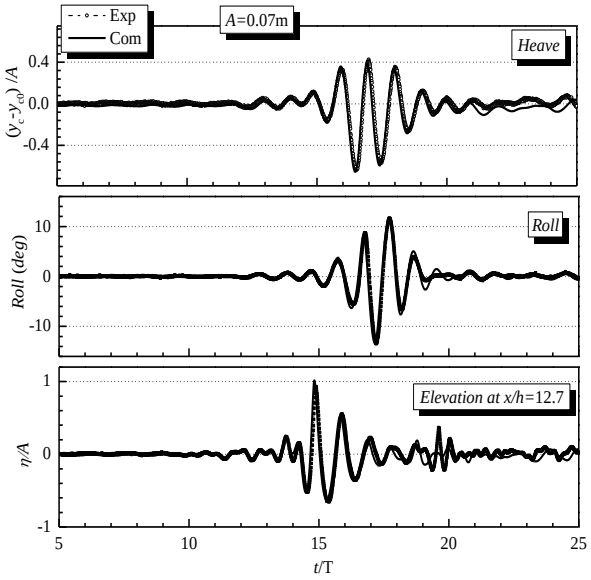

Fig. 9 2-DOF body motions due to focused waves.

3--DOF body motions

In this section, results are presented for 3-DOF body motions. The sway motion is restrained by a spring with a spring constant of 3.82N/m. Figs. 10-12 show the results for 3-DOF case. The computed body responses agree well with the experimental results. Meanwhile, the results for heave, pitch and wave elevation are similar to those obtained in the fixed-sway case in Figs.7-8. Look

closely, the computational results show a slight discrepancy at the end of simulation. It mainly caused by the complex water-air-body nonlinear interactions at the last stage of green water phenomena, including wave breaking, water-air mixing. As shown in Fig. 12, the numerical simulation of the pressure field and the velocity vector around the body at different times is presented. The results reveal the focused wave collides with the offshore structure and the pressure and velocity abruptly changes around the structure. The result at t=20.0s reveals that before the wave approach the body, the velocity is less complicated. After that, the body starts to move on the offshore direction and it is about to rotate in clockwise direction, as seen at t=20.2s. With time increases, the green water happens and slams on the superstructure. It is very similar for the two cases: 2-DOF and 3-DOF. The detailed green water impact phenomena can be found in Fig. 7. At t= 20.4s, the body starts to rotate in anticlockwise direction and is seen to reach its maximum value after t=20.6s. Here, it should be pointed that the main feature is the water-air-body nonlinear interactions caused by the fall of the green water from t=20.6s and t=20.8s. Also, vortexes appear under the side bottom corner of the body. It can be found the extremely nonlinear phenomena like violent impact, wave breaking, water-air mixing and vortex shedding can be captured by the present CFD model.

CONCLUSIONS

In the present paper, a two-dimensional numerical model of calculating response of 2-D floating structure due to the focused wave is investigated numerically and experimentally. We paid our attention to the 3-DOF motions of the floating structure, the green water phenomena and impact pressure. The comparison between the numerical and the experimental results regarding the water surface elevations, dynamics responses of the floating body, impact pressure due to green water confirms the validity of the present numerical model. Numerical investigation demonstrates that the present CFD model is capable of predicting the impact of extreme waves on a floating structure, which is of great importance to the real ocean engineering applications.

ACKNOWLEDGEMENTS

The laboratory experiments of this paper were carried out during X. Zhao's visit to the RIAM of Kyushu University. Financial support from Kyushu University for X. Zhao is gratefully acknowledged. This work is jointly supported by the Fundamental Research Funds for the Central Universities (2012QNA4020), the National Natural Science Foundation of China (No. 51209184) and the Zhejiang Open Foundation of the Most Important Subjects.

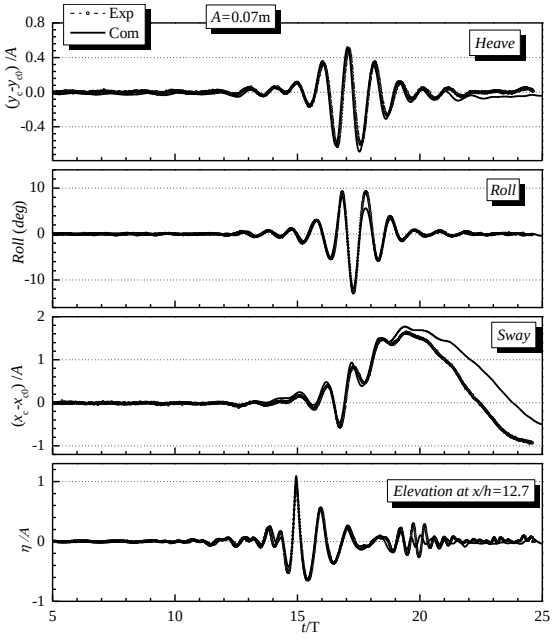

Fig. 10 3-DOF body motions due focused waves

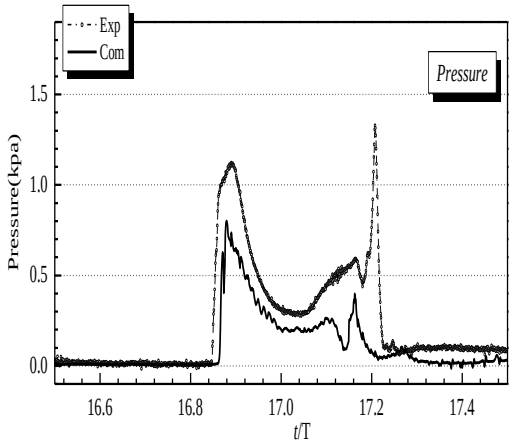

Fig. 11 Impact pressure due to green water

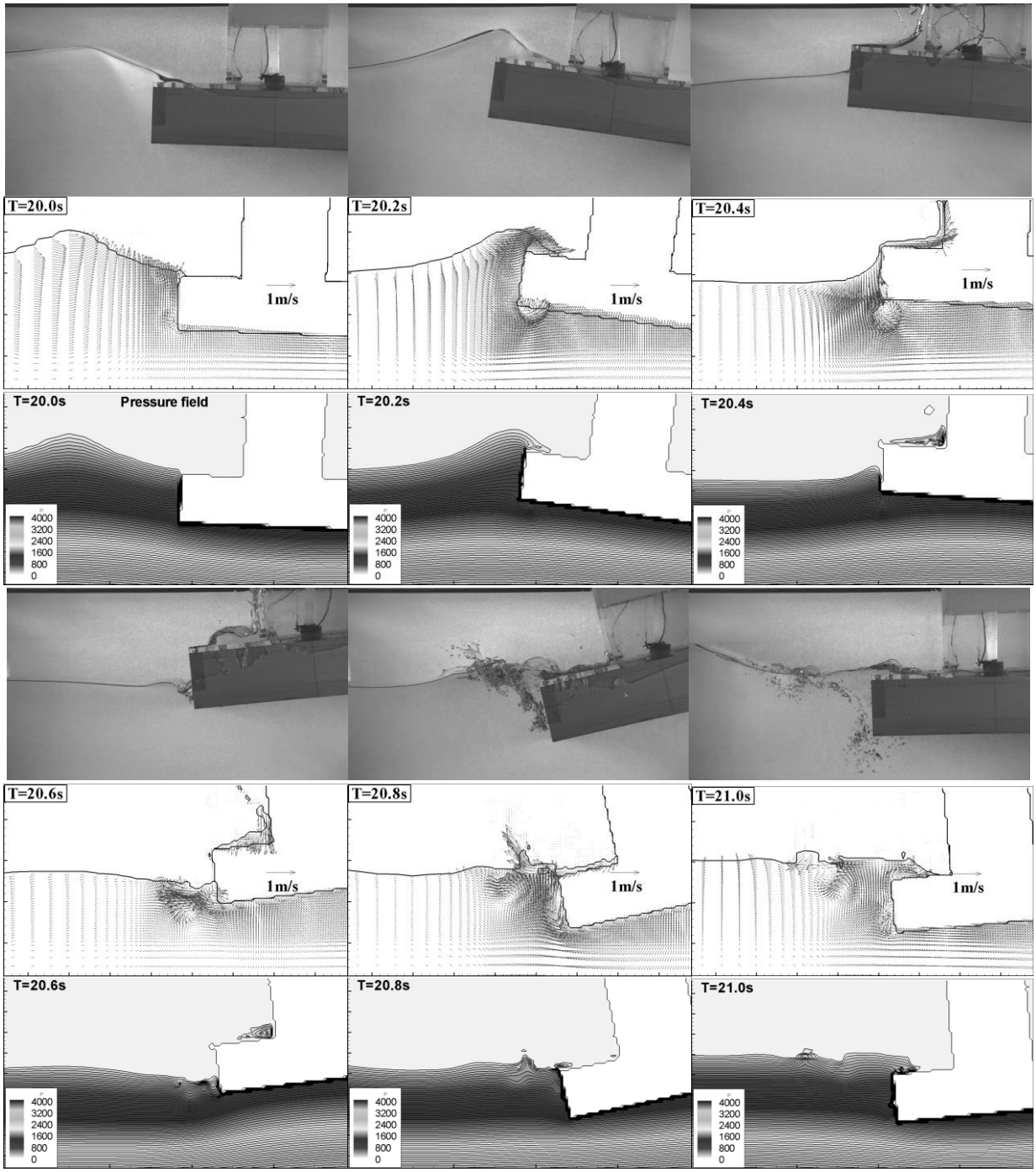

Fig. 12 Pressure field, velocity vector and free surface around the body during the impact progress with 3-DOF

REFERENCES

Davis, M.C. and Zarnick, E.E. (1964). Testing ship models in transient waves. Proceedings of the 5th International Symposium on Naval Hydrodynamics. Washington, DC, Office of Naval Research, 509-540.

Draper, L. (1965). 'Freak' wave. Marine Observer 35: 193-195.

Dysthe, K., Krogstad, H.E. and Muller, P. (2008). Oceanic rogue waves. Annu. Rev. Fluid Mech., 40: 287-310.

Hirt, C.W. and Nichols, B.D. (1981). Volume of fluid (VOF) method for the dynamics of free surface boundaries. J. Comput. Phys., 39: 201-25.

Hu, C.H. and Kashiwagi, M. (2004). A CIP-based method for numerical simulations of violent free surface flows. J. Mar.Sci. Technol., 9: 143-157.

Hu, C.H. and Kashiwagi, M. (2009). Two-dimensional numerical simulation and experiment on strongly nonlinear wave-body interactions. J. Mar. Sci. Technol., 14(2): 200-213.

Hu, Z.Z., Causon, M., Mingham, C.G. and Qian, L. (2011). Numerical simulation of floating bodies in

extreme free surface waves. Nat. Hazard. Earth Sys., 11: 519-527.

Huang, Z.L. and Lin, P.Z., 2012. Numerical simulation of propagation and breaking processes of a focused waves group. J. Hydrodyn., 24 (3): 399-409.

Kharif, C. and Pelinovsky, E. (2003). Physical mechanisms of the rogue wave phenomenon. Eur. J. Mech-B/Fluid., 22: 603-634.

Li J.X. Wang Z.H. and Liu, S.X. (2012). Experimental study of interactions between multi-directional focused wave and vertical circular cylinder, Part I: Wave run-up. Coastal Eng., 64: 151-160.

Liu, S.X., Sun, Y.Y., Li, J.X. et al. (2010). Experimental study on 2-D focusing wave run-up on a vertical cylinder. China Ocean Eng., 24 (3): 499-512.

Longuet-Higgins, M.S.(1952). On the statistical distribution of the heights of sea waves. J. Mar. Res., 11: 245-266.

Nikolkina, I. and Didenkulova, I. (2011). Rogue waves in 2006-2010. Nat. Hazard. Earth Sys., 11: 2913-2924.

Westphalen, J., Greaves, D.M., Williams, C.J.K. et al. (2012). Focused waves and wave-structure interaction in a numerical wave tank. Ocean Eng., 45: 9-21.

Xiao, F., Honma, Y. and Kono, T., (2005). A simple algebraic interface capturing scheme using hyperbolic tangent function. Int. J. Numer. meth. Fluids, 48: 1023-1040.

Xiao, F., Ii, S. and Chen, C. (2011). Revisit to the THINC scheme: a simple algebraic VOF algorithm. J. Comput. Phys., 230:7086-7092.

Yabe, T., Xiao, F. and Utsumi, T. (2001). The constrained interpolation profile method for multiphase analysis. J. Comput. Phys., 169(2): 556-593.

Yokoi, K. (2007). Efficient implementation of THINC scheme: a simple and practical smoothed VOF algorithm. J. Comput. Phys., 226: 1985-2002.

Youngs, D.L. (1982). Time-dependent multi-material flow with large fluid distortion. Numerical Methods for Fluid Dynamics, Edited by Morton, K.W., Baines, M.J., 24:273-285.

Zhao, X.Z. (2011). Validation of a CIP-based tank for numerical simulation of free surface flows. Acta Mech. Sinica, 27(6): 877-890.

Zhao, X. and Hu, C. (2012). Numerical and experimental study on a 2-D floating body under extreme wave Conditions. Appl. Ocean Res., 35: 1-13.

Zhao, X., Hu, C. and Sun, Z.(2010a). Numerical simulation of extreme wave generation using VOF method. J. Hydrodyn., 22(4): 466-477.

Zhao, X., Sun, Z. and Liang, S. (2010b). Effects of wave breaking on freak wave generation in random wavetrain. China Ocean Eng., 24(4): 653-662.

Zhao, X., Sun, Z. and Liang, S. (2009). Efficient focusing models for generation of freak waves. China Ocean Eng., 23(3): 429-440.

Zhao, X. and Dong, Sh. (2011). Numerical simulation of extreme wave impact on a floating body with experimental validation. Proc. 6th International Conference on APAC, Hongkong, 1668-1675.

Zalesak, S.T. (1979). Fully multi-dimensional flux corrected transport algorithm for fluid flow. J. Comput. Phys., 31: 35-62.

Zang, J., Taylor, P.H. and Tello, M. (2010). Steep wave and breaking wave impact on offshore wind turbine foundations-ringing revisited. Proc. 25th IWWWF, Harbin, China.